Calibration of UAS imagery inside and outside of shadows for improved vegetation index computation

Elizabeth Bondi, Carl Salvaggio, Matthew Montanaro, and Aaron D. Gerace

Rochester Institute of Technology, Chester F. Carlson Center for Imaging Science, Digital Imaging and Remote Sensing Laboratory, 54 Lomb Memorial Drive, Rochester, NY, USA

ABSTRACT

Vegetation health and vigor can be assessed with data from multi- and hyperspectral airborne and satellite-borne sensors using index products such as the normalized difference vegetation index (NDVI). Recent advances in unmanned aerial systems (UAS) technology have created the opportunity to access these same image data sets in a more cost effective manner with higher temporal and spatial resolution. Another advantage of these systems includes the ability to gather data in almost any weather condition, including complete cloud cover, when data has not been available before from traditional platforms. The ability to collect in these varied conditions, meteorological and temporal, will present researchers and producers with many new challenges. Particularly, cloud shadows and self-shadowing by vegetation must be taken into consideration in imagery collected from UAS platforms to avoid variation in NDVI due to changes in illumination within a single scene, and between collection flights. A workflow is presented to compensate for variations in vegetation indices due to shadows and variation in illumination levels in high resolution imagery collected from UAS platforms. Other calibration methods that producers may currently be utilizing produce NDVI products that still contain shadow boundaries and variations due to illumination, whereas the final NDVI mosaic from this workflow does not.

Keywords: calibration, shadow detection, empirical line method, unmanned aerial systems, reflectance

1. INTRODUCTION

In traditional remote sensing from aircraft or satellite-based sensors such as Landsat, shadows from trees and clouds have negligible influence, due to the large ground sampling distance (GSD) of sensors on these platforms, when the data is used to assess vegetation health. Unlike satellite or aircraft imagery, the pixel size from UAS platforms is on the order of centimeters. This provides great benefits for measuring crop health because smaller trouble areas can be spotted. Unfortunately, this increased spatial resolution causes problems. Small changes in illumination caused by clouds or shadows can play an influential role in the determination of vegetation health. Additionally, the UAS can be flown at any time of the day. Because of these new factors, even if the reflectance of the vegetation in two locations is the same, the sensor-reaching radiance will be different.

To measure vegetation health, an index known as normalized difference vegetation index (NDVI) is often used. NDVI is a metric that has been utilized to measure vegetation health since 1973.[1] It is traditionally calculated from the radiance of the red and infrared bands of multispectral image data as

$$NDVI = \frac{L_{IR} - L_R}{L_{IR} + L_R} \tag{1}$$

where L_{IR} and L_R are the ground-leaving radiance in the infrared and red bands, respectively, recorded at each image location.

To illustrate the fact that NDVI calculated from radiance will change due to shadows and clouds, MODTRAN 4v3r1[2] was used to model the ground-reaching radiance, path radiance, and sensor-reaching radiance for imagery taken in Rochester, NY, USA on a cloudy day (cumulus clouds) at noon and a clear day at noon. The sensor-reaching radiance is shown in Fig. 1. The integrated bandpass radiance was computed using the spectral transmission for the filters of a multispectral camera (Tetracam Micro-MCA6 Global SNAP), shown in Fig. 2.

Further author information: (Send correspondence to Carl Salvaggio, E-mail: salvaggio@cis.rit.edu)

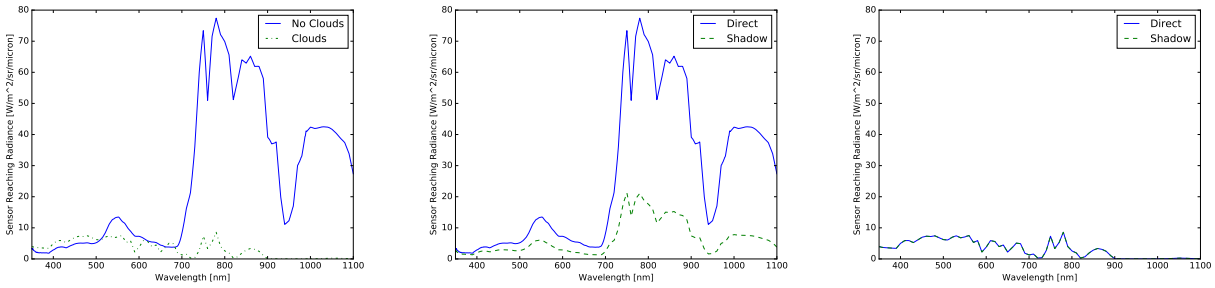

(a) (b) (c)

Figure 1: The sensor-reaching radiance, including both cloudy and not cloudy, as well as shadowed and directly-lit regions. From left to right: no clouds and clouds, directly illuminated, 12PM (1a); no clouds, directly illuminated and shadowed, 12PM (1b); clouds, directly illuminated and shadowed, 12PM (1c).

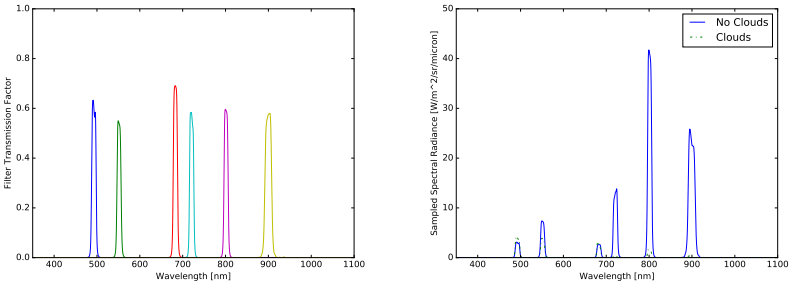

(a) (b)

Figure 2: Filter transmissions[3] (2a) and spectrally sampled radiance (2b), calculated by multiplying the filter transmissions by the sensor-reaching radiance (Fig. 1a).

NDVI was calculated using the integrated bandpass radiance values for the Tetracam bands centered at 800 and 680 nm, producing the results summarized in radiance column of Table 1. Although the same reflectance spectrum for healthy vegetation was used for each simulation, the different illumination conditions produced different NDVI values. The radiance in the infrared region of the spectrum was attenuated by the cumulus clouds, which led to a lower NDVI value. Shadows were modeled using skylight illumination only, and a similar phenomenon was observed when shadows were present.

To compensate for the varying levels of illumination and shadow depicted previously, reflectance was derived from the integrated radiances through the use of simulated calibration panels of known reflectance, both in and out of shadow. Reflectance was presumed to be an illumination invariant value for a fixed observation location, and the empirical line method (ELM) was used to convert from radiance to reflectance using the known reflectance of the panels.[4] These results are also shown in Table 1.

Table 1: NDVI calculated from radiance and reflectance using different ephemeral imaging conditions.

Conditions	NDVI (from radiance)	NDVI (from reflectance)
12PM, No Clouds	0.89	0.92
12PM, No Clouds, Shadows	0.86	0.92
12PM, Clouds	-0.21	0.92
12PM, Clouds, Shadows	-0.21	0.92

Since the sensor-reaching radiance will be different at different collection times or within shadows and clouds, different NDVI values will be calculated even if the vegetation has not changed it biotic condition. To compensate for these issues, calibration panels, either shadowed or directly illuminated, can be used to convert sensor-reaching radiance into target reflectance. This removes the effects of varying illumination on NDVI.

2. BACKGROUND

2.1 Vegetation Indices

As mentioned in Section 1, NDVI is an index used to quantify the health of vegetation using radiance, digital counts, or diffuse hemispheric reflectance (hereinafter reflectance) as input parameters. Regardless of the quantity used, this vegetation index is based on the principle that the infrared region of vegetation's reflectance spectrum correlates to the amount of chlorophyll in the target sampled, and that the red region of the reflectance spectrum remains relatively constant. For healthy vegetation, the red reflectance tends to be low, and the infrared reflectance tends to rise dramatically, leading to NDVI values approaching one.[4] This works well for satellite imagery, but it is not completely invariant when radiance or digital counts are used. Therefore, the primary goal of the approach was to use reflectance, ρ, to compute NDVI (Eq. 2) in order to remove the invariance introduced by using radiance or digital counts in this process.

$$NDVI = \frac{\rho_{IR} - \rho_R}{\rho_{IR} + \rho_R} \tag{2}$$

2.2 Empirical Line Method

To convert radiance into reflectance to calculate NDVI from data collected by UAS, one of the simplest approaches is to use the Empirical Line Method (ELM). By using large, Lambertian calibration panels of known reflectances at the time of data collection, linear regression can be used to convert digital count to reflectance for each band, assuming the radiance is linearly related to the digital counts reported by the camera.[4] The size of the panels needs to be several times larger than the ground instantaneous field-of-view, smooth, flat in appearance, and level to the ground for the best results.[5]

2.3 Shadow detection

If converting to reflectance using a calibration target that is fully illuminated, shadow inconsistencies may still be unaccommodated. The addition of calibration panels in shadow regions will increase the accuracy of the NDVI images produced from UAS data. Specifically, the addition of shadowed calibration panels could be used for ELM in shadowed regions instead of fully illuminated panels.

Although there are many methods for shadow detection, one of the simplest methods is that of Otsu.[6] In this method, a bimodal histogram is "split" based on variance metrics. Any digital count below the identified threshold is categorized as one class, and anything above the threshold is categorized as a second class. This can be used for shadow detection, where everything below the threshold is shadow, and everything above the threshold is considered directly illuminated.

3. METHODOLOGY

The purpose of this study was to take multispectral UAS imagery and derive NDVI mosaics of agricultural fields that are consistent under multiple levels of illumination. The workflow to create NDVI mosaics is illustrated in Fig. 3. The steps in the workflow were data collection involving shaded and sunlit calibration panels, digital count to reflectance look-up table (LUT) generation using ELM, shadow detection, LUT application based upon the shadow classification of each pixel, orthomosaicking of the resultant reflectance images, and finally NDVI calculation on the reflectance mosaic. A Tetracam Micro-MCA6 Global SNAP was flown for all collections conducted as part of this research.

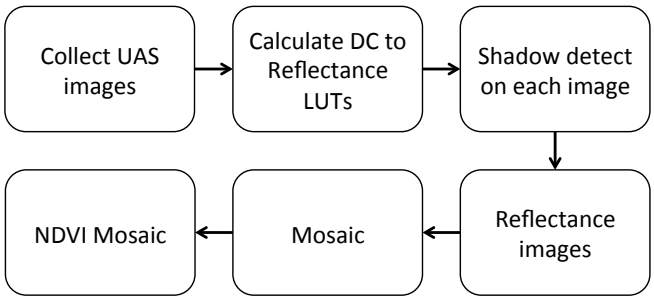

Figure 3: Illustration of the workflow used to create NDVI mosaics from UAS imagery.

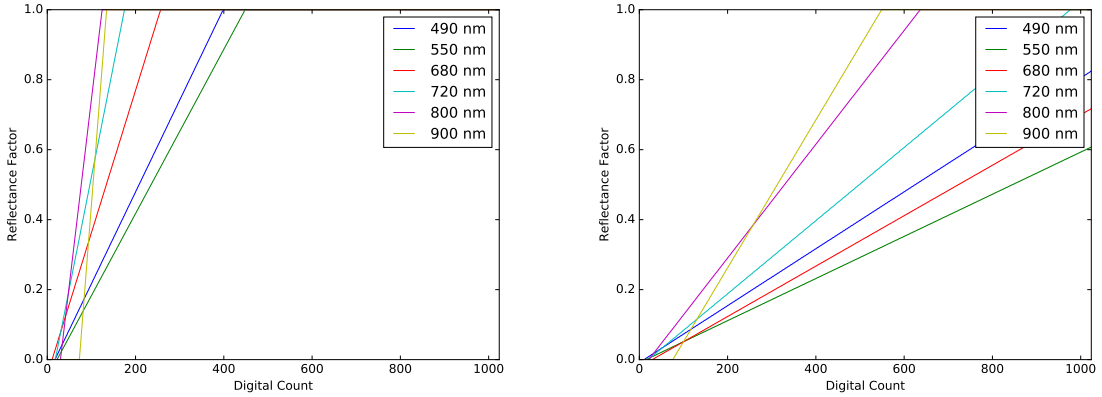

(a) (b)

Figure 4: LUT from digital count to reflectance for a single image, with all bands; shadow LUT (4a), directly illuminated LUT (4b).

3.1 DC-to-Reflectance LUTs

During a typical UAS collection mission utilized for this study, several hundred six-band images were collected. At the end of each flight line, the light and dark panels were positioned such that a calibration curve could be computed for every transect to mitigate changes in illumination during the collection mission. Several of these images had directly illuminated ELM panels, several had shadowed ELM panels. For each image containing a panel, the mean digital count and standard deviation in a region of interest surrounding the panel were recorded. Six reflectance values were derived for each panel by integrating the reflectance spectra over the bandpass for each of the six image bands.

With this information, a digital count-to-reflectance LUT could be created for each band (Fig. 4). Eq. 3 was used to relate digital count (DC) to reflectance (ρ), where m is the slope, and b is the y-intercept of a linear fit. A LUT for conversion of each DC to reflectance could then be constructed. Eq. 4 and Eq. 5 were used to calculate m and b for each band in the image, where the subscripts l and d denote the usage of light and dark panels for the parameters, respectively. Note that linear interpolation based on image time was carried out to estimate the LUT for images that did not contain panels.

$$\rho = m(DC) + b \tag{3}$$

$$m = \frac{\rho_l - \rho_d}{DC_l - DC_d} \tag{4}$$

$$b = \rho_l - (mDC_l) \tag{5}$$

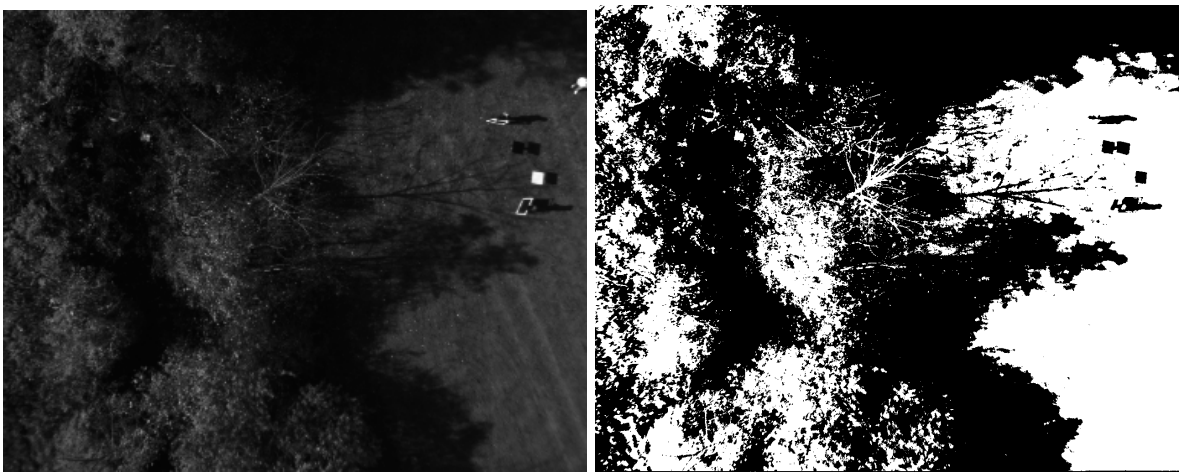

(a) (b)

Figure 5: Green (550 nm) band of one image collected (5a). This image contains directly illuminated ELM panels (upper right). Shadow map of 5a (5b).

3.2 Shadow Detection

By doing shadow detection on an image to determine which pixels were shadowed or directly illuminated, the corresponding LUTs could be assigned on a pixel-by-pixel basis. Otsu's thresholding was used for shadow detection as discussed in Section 2.3 and the resulting shadow map is shown in Fig. 5b. It is evident in the figure that there were some misclassified pixels, particularly on the calibration panels in the upper right corner. The dark panel was sunlit, but because it was one of the darker objects in the scene, therefore it was errantly classified as a shadow.

3.3 Reflectance, Reflectance Mosaic and NDVI Mosaic

The appropriate LUT was applied on a per-pixel basis, to every mission image, after shadow detection was completed. This yielded a collection of six-band reflectance images. The reflectance images were then orthomosaicked using Agisoft's Photoscan Pro to create a six-band reflectance orthomosaic. The NDVI orthomosaic was then calculated by using Eq. 2. For ρ_{IR}, the band corresponding to 800 nm was used, and for ρ_R, the band corresponding to 680 nm was used. The resulting derived orthomosaic contained a single band with floating point values ranging from -1.0 to 1.0. It was displayed so green represents an NDVI close to 1.0, and red represents an NDVI less than or equal to 0.0.

4. RESULTS

The NDVI mosaics generated using this workflow for both the sunny and cloudy days have been included in Fig. 6d and Fig. 7c, respectively. The shadowed areas do not have noticeable boundaries. The other NDVI mosaics in these plots have been generated by using other calibration methods that producers may currently be utilizing. For example, Fig. 6b was created by using a radiometric calibration that converted digital count to radiance. As is evident by looking at the shadowed areas of the mosaic, NDVI derived from radiance yielded incorrect results. On the sunny day, simply converting everything to reflectance based on a single LUT also yielded incorrect results, particularly in the shadowed areas (Fig. 6c). By only using digital counts, the results were even more inconsistent (Fig. 6a).

The primary deficiencies remaining with this workflow are the shadow detection efficacy, calibration panel shadowing in the field, and remaining inconsistencies in NDVI between sunny and cloudy days. Shadow detection could be improved with a more sophisticated method and the calibration panels could use a more transmissive, leaf-like fabric to create shade. The remaining inconsistencies are likely due to multiple scattering effects[7] due to the collection geometry variation between the two collections, and could likely be removed by keeping the

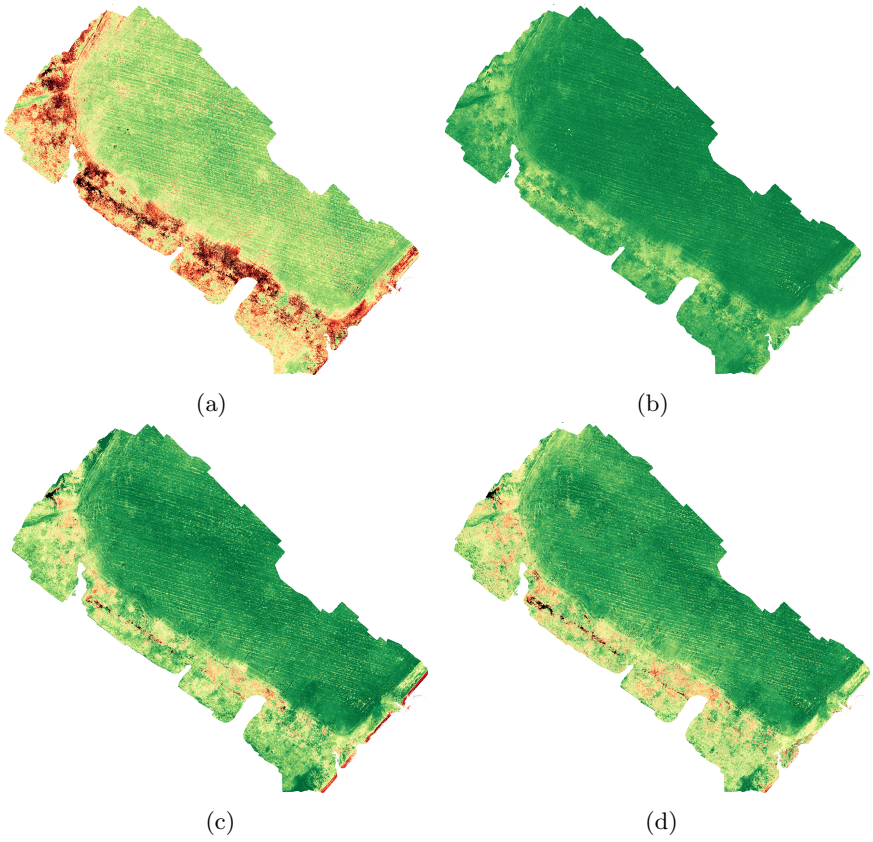

Figure 6: Normalized difference vegetation index (NDVI) orthomosaic images created using raw digital count data (6a), calibrated at-sensor radiance (6b), ground reflectance obtain using only sunlit-derived digital count-to-reflectance calibration tables (6c), and ground reflectance obtain using sun/shadow digital count-to-reflectance calibration tables (6d)

collection geometry consistent between multiple flights. A more thorough analysis of the performance of this calibration procedure is also necessary. This could include error propagation throughout the LUT generation process, and comparison to ground truth NDVI derived from ground spectroradiometric measurements.

5. CONCLUSIONS

The workflow presented in this study is the first step towards creating temporally consistent NDVI from UAS imagery. There are still several problems, including shadow detection, calibration panel shadowing in the field, and a lack of consideration for multiple scattering, that need to be addressed. Despite these remaining deficiencies, one can see the marked increase in accuracy that is obtained using the calibration process described.

ACKNOWLEDGMENTS

The authors would like to express their heartfelt thanks to Pegasus Ecological, Ltd., Zeke Hurd and "Papa" Jeff Ring, for their mentorship and assistance in UAS integration and flight in support of this effort.

REFERENCES

1. J. Rouse Jr., R. Haas, J. Schell, and D. Deering, "Monitoring vegetation systems in the Great Plains with ERTS," *NASA Special Publication* **351**, p. 309, 1974.

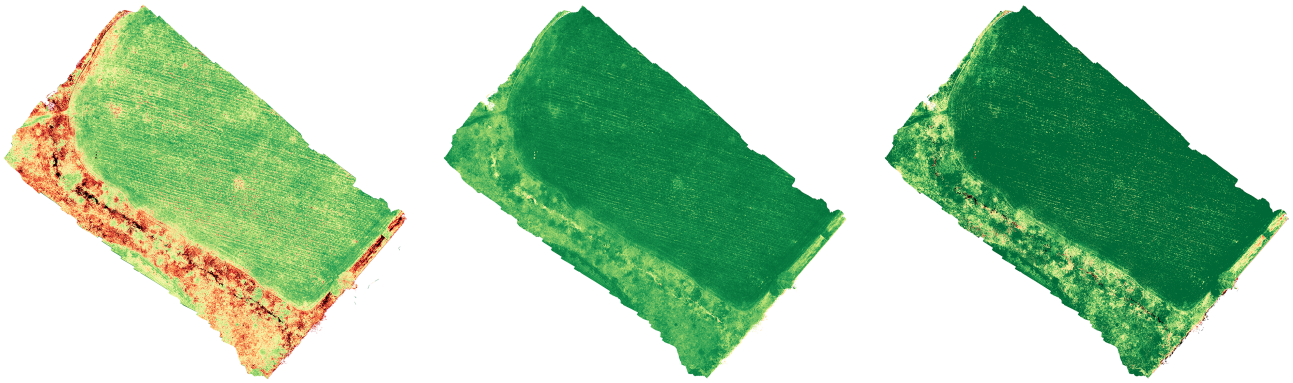

(a) (b) (c)

.

Figure 7: Normalized difference vegetation index (NDVI) orthomosaic images created using raw digital count data (7a), calibrated at-sensor radiance (7b), and ground reflectance obtain using only shadow-derived digital count-to-reflectance calibration tables (7c)

2. G. P. Anderson, A. Berk, P. K. Acharya, L. S. Bernstein, S. M. Adler-Golden, J. Lee, and L. Muratov, "Reformulated atmospheric band model method for modeling atmospheric propagation at arbitrarily fine spectral resolution and expanded capabilities.," 2009. U.S. Patent 7,593,835.
3. "Andover Corporation 193-299 nm Standard Bandpass Optical Filters," Available at https://www.andovercorp.com/products/bandpass-filters/standard/193-299nm/.
4. J. R. Schott, *Remote Sensing - The Image Chain Approach*, Oxford University Press, 2007.
5. G. M. Smith and E. J. Milton, "The use of the empirical line method to calibrate remotely sensed data to reflectance," *International Journal of Remote Sensing* **20**(13), pp. 2653–2662, 1999.
6. N. Otsu, "A threshold selection method from gray-level histograms," *Automatica* **11**(285-296), pp. 23–27, 1975.
7. J. Widlowski, C. Mio, M. Disney, J. Adams, I. Andredakis, C. Atzberger, J. Brennan, L. Busetto, M. Chelle, and G. Ceccherini, "The fourth phase of the radiative transfer model intercomparison (RAMI) exercise: Actual canopy scenarios and conformity testing," *Remote Sensing of Environment* **169**, pp. 418–437, 2015.